AGU PUBLICATIONS

Geophysical Research Letters

RESEARCH LETTER
10.1002/2014GL061310

Key Points:
- Regular 26 min inflation/deflation cycles are observed at silicic volcano
- Inflation rates control whether volcano explodes or passively degasses
- Location of gas reservoir and flux of gas through the volcano are quantified

Supporting Information:
- Readme
- Table S1
- Movie S1
- Movie S2
- Movie S3
- Movie S4

Correspondence to:
J. B. Johnson,
jeffreybjohnson@boisestate.edu

Citation:
Johnson, J. B., J. J. Lyons, B. J. Andrews, and J. M. Lees (2014), Explosive dome eruptions modulated by periodic gas-driven inflation, *Geophys. Res. Lett.*, *41*, 6689–6697, doi:10.1002/2014GL061310.

Received 24 JUL 2014
Accepted 4 SEP 2014
Accepted article online 5 SEP 2014
Published online 3 OCT 2014

Explosive dome eruptions modulated by periodic gas-driven inflation

Jeffrey B. Johnson[1], J. J. Lyons[2], B. J. Andrews[3], and J. M. Lees[4]

[1]Department of Geosciences, Boise State University, Boise, Idaho, USA, [2]Alaska Volcano Observatory, USGS, Anchorage, Alaska, USA, [3]Department of Mineral Sciences, Smithsonian Institution, Washington, District of Columbia, USA, [4]Department of Geological Sciences, University of North Carolina, Chapel Hill, North Carolina, USA

Abstract Volcan Santiaguito (Guatemala) "breathes" with extraordinary regularity as the edifice's conduit system accumulates free gas, which periodically vents to the atmosphere. Periodic pressurization controls explosion timing, which nearly always occurs at peak inflation, as detected with tiltmeters. Tilt cycles in January 2012 reveal regular 26 ± 6 min inflation/deflation cycles corresponding to at least ~10^1 kg/s of gas fluxing the system. Very long period (VLP) earthquakes presage explosions and occur during cycles when inflation rates are most rapid. VLPs locate ~300 m below the vent and indicate mobilization of volatiles, which ascend at ~50 m/s. Rapid gas ascent feeds pyroclast-laden eruptions lasting several minutes and rising to ~1 km. VLPs are not observed during less rapid inflation episodes; instead, gas vents passively through the conduit producing no infrasound and no explosion. These observations intimate that steady gas exsolution and accumulation in shallow reservoirs may drive inflation cycles at open-vent silicic volcanoes.

1. Introduction

Santiaguito in Guatemala provides the ideal laboratory for study of eruption dynamics of a relatively silicic (64–72 wt % [*Scott et al*., 2013]) system, similar in morphology and chemistry to other well-known and recently active domes including Unzen (Japan), Soufrière Hills (Montserrat), Bezymianny (Russia), and Mount St. Helens (USA) [*Siebert and Simkin*, 2002]. The eviscerated parent edifice of Santa Maria, which erupted in 1902, provides a bird's-eye perspective as it rises 1200 m above and only 2700 m distant from the active Caliente vent (Figure 1). Santiaguito is considered a "partially open-vent system" because, although its lava effusion is continuous, explosive eruptions are intermittent, suggesting at least temporary sealing of gas pathways [e.g., *Holland et al*., 2011]. Such episodic eruptive behavior is characteristic of many long-lived active, "open-vent" andesitic and dacitic volcanoes worldwide, including Colima (Mexico), Karymsky (Russia), and Sakurajima (Japan) [*Siebert and Simkin*, 2002].

Santiaguito's activity has been continuous at its Caliente vent since 1968 and regular ~ hourly explosions have been common since at least the early 1970s [*Rose*, 1987]. These explosions have been accompanied by an effusive lava flux that has varied from ~0.1 m^3/s to 0.7 m^3/s [*Harris et al*., 2002] but has probably never completely stopped. In the most recent decade, explosions have emanated from ephemeral arcuate fractures distributed over a broad (~30,000 m^2) summit plateau and are well observed from the summit of Santa Maria [e.g., *Bluth and Rose*, 2004; *Sahetapy-Engel et al*., 2008; *Johnson et al*., 2008].

2. Study

In January 2012 geophysical instruments were deployed on a level expanse, which extends to within ~500 m NE of the Caliente vent. Deployment proximity allowed exceptional sampling of near-field deformation, which falls off rapidly as $1/r^2$. Nearness is critical for good signal to noise for the short baseline platform tiltmeters (Applied Geomechanics 700 series) and for recovery of near-field very long period (VLP) seismic displacements using broadband seismometers (Nanometrics Trillium Compact and Guralp CMG-40 T). Tilt, seismic, and infrasound sensors were continuously recorded at 100 Hz using Reftek RT130 loggers with GPS time synchronization. Data were compared with optical band time-lapse camera imagery taken from Santa Maria's summit (Figure 2).

Conjoint tilt-seismic-infrasound and video illuminate internal conduit dynamics and their linkage to surface activity. This study is the first to observe that the Caliente edifice periodically inflates, as indicated by radially oriented tilt on two tiltmeters. Moreover, observations show that as the tilt nears peak inflation, the system either

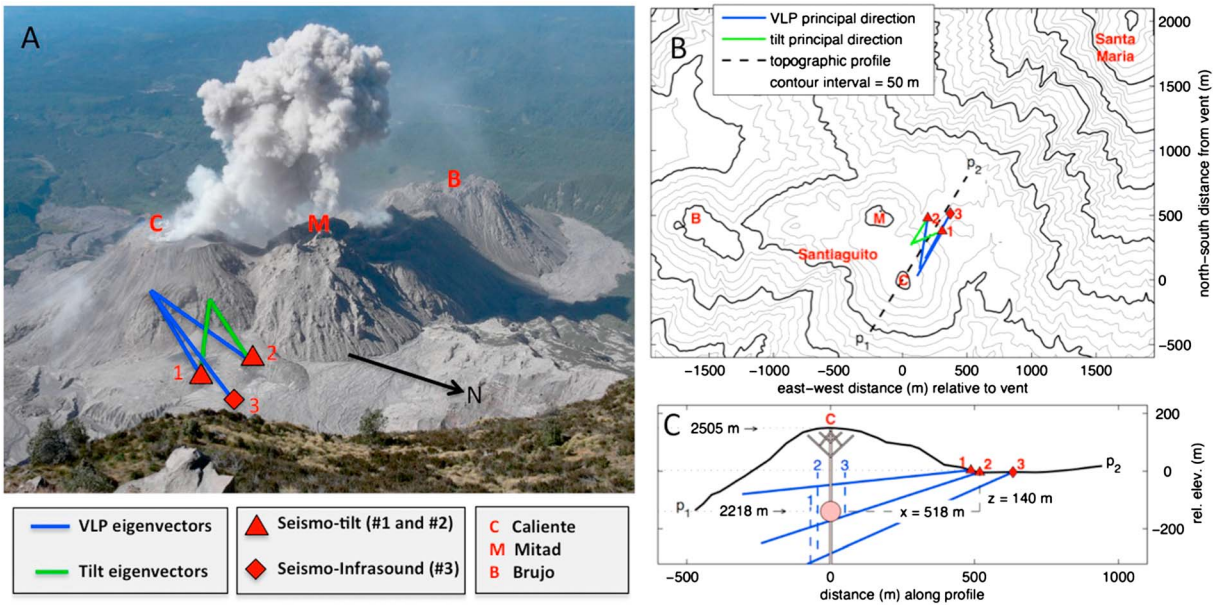

Figure 1. (a) View from Santa Maria and (b) corresponding topographic map. Location of domes (C, M, and B), as well as array sensor deployment, is indicated. Intersecting blue and green lines correspond, respectively, to principal tilt and VLP seismic oriented nearly radial toward an inferred conduit. (c) Profile shows VLP particle motion principal direction (solid blue lines) and range of potential source depths for each station (blue dashed lines). Overlap region is used as the VLP source region (pink circle) and is at $z = 140$ m referenced to the mean station elevation.

culminates in an explosion (as indicated by the presence of an infrasound pulse, VLP signal, and rapid tilt deflation, e.g., events 1, 2, 5, 7 in Figure 2). Or, alternatively, the volcano deflates benignly without explosion or apparent VLP.

Nighttime time-lapse imagery qualitatively shows that heightened gas emissions correlate with tilt cycles even when explosive degassing is absent (Figures 2g and 2h). Proxy for gas emissions is inferred from median red color intensity in time-lapse images; i.e., when fume is present, the red glow refracting off the incandescing dome is more intense. This time-lapse imagery also shows fluctuations in lava effusion as evidenced by bulging of the lava surface quantified with particle image velocimetry (PIV) [*Johnson et al.*, 2013] (e.g., see Figure 2a); however, these surface distensions are not associated with the tilt cycles. Because tilt cycles are correlated with the degassing proxy, which consistently lags inflation by ~5 min (Figures 2g and 2h), we conclude that it is gas accumulation and venting that largely drives the observed tilts. Peak gas emissions coincide with deflationary tilt. This results from gas fluxing up through the upper conduit and in to the atmosphere.

Fluctuating gas emissions were observed during Santiaguito studies in 2008 and 2009 using UV imagers that detect SO_2 flux [*Holland et al.*, 2011]. Cyclic emissions shown in Figure 3 of *Holland et al.* [2011] correspond to both explosions and nonexplosive elevated degassing occurring about every 30 min. Their timing is consistent with our observed 26 min degassing interval. Our cycles also reflect both explosive and nonexplosive emissions, which are observed through optical observations of elevated fume.

We borrow from key aspects of the *Holland et al.* [2011] model to explain our seismogeodetic, infrasound, and visual observations. In particular, our data are consistent with pressure sources originating in a region several hundred meters below the vent as located by *Sanderson et al.* [2010]. This is hypothesized as a region where the conduit becomes intermittently impermeable, i.e., where "fracture healing occurs by viscous relaxation" over tens of minutes time scales [*Holland et al.*, 2011]. Further, our observations corroborate that explosive gas flow permeates upward from this region through a "continuous network of small-scale fractures." Our geophysical constraints build upon the *Holland et al.* [2011] model to provide chronology and magnitude for internal pressurization and flow dynamics.

3. Anatomy of an Explosion (Seismogeodetic Constraints)

Detail of explosion signals show emergence of a VLP (Figure 3, a) ~6 s prior to the explosion of gas at the surface (as detected by conjoint infrasound and tilt inflection; Figure 3, b). VLPs are long wavelength

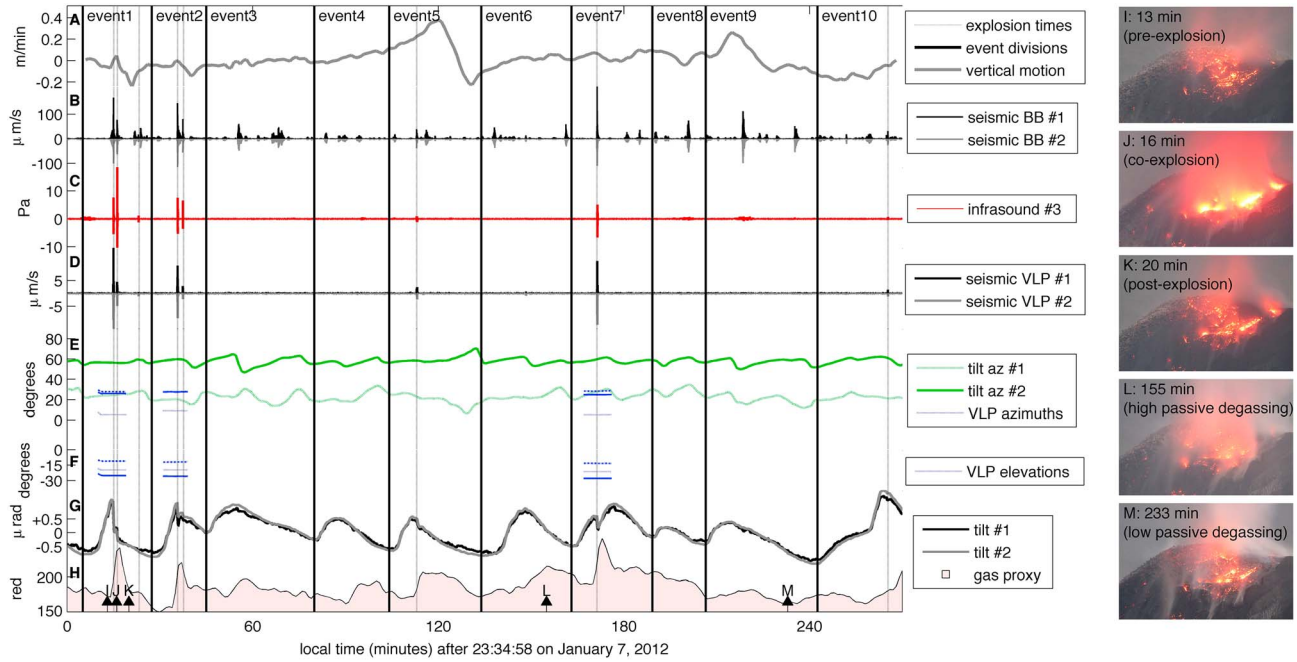

Figure 2. Joint geophysical observations from 4.5 h of typical Santiaguito activity are described. (a) Average vertical velocity of dome surface calculated using PIV [*Johnson et al.*, 2013], (b) broadband (BB; 0.05 to 20 Hz) composite vertical seismic shown for stations #1 (positive polarity; black) and #2 (negative polarity; grey) indicating both explosion and rock fall signals. (c) Infrasound (filtered above 0.25 Hz) pressure transients showing the occurrence of explosive degassing for cycles #1, 2, 5, and 7 (also indicated by vertical dashed lines). (d) VLP-filtered (0.05 to 0.2 Hz) seismic velocity records showing signal associated with explosions. (e) Principal azimuths of the short-duration rectilinear VLP signals and of tilt, for which the median directions are indicated in Figure 1. (f) Elevation angle (relative to horizontal) of VLP principal components. (g) Tilt records from two stations along with (h) gas flux proxy comparison, qualitatively extracted from red color band median intensity. (i–m) Nighttime images of the active dome surface for indicated times. Relatively low degassing periods (Figures 2i, 2k, and 2m). Heightened degassing associated with VLP inflation (Figure 2j) and non-VLP inflation (Figure 2l), respectively. Note that the animations of time-synced infrasound, seismic, tilt, and time-lapse footage for this time interval are provided as dynamic content in the supporting information.

elastostatic deformations observed in conjunction with explosions at many diverse open-vent volcanoes, e.g., Stromboli (Italy) or Erebus (Antarctica), and are thought to be associated with volumetric changes internal to the volcano edifice [*Neuberg et al.*, 1994; *Rowe et al.*, 1998]. Principle component VLP particle motions may point to the locus of volume change, so long as care is taken to account for oblique incidence of seismic waves at the free surface [*Neuberg and Pointer*, 2000]. We apply a range of potential body wave velocity ratios ($1.55 < V_P/V_S < 1.8$) to determine potential *P* wave incidence directions. For stations #1–3, we use the 0.05 to 2 Hz band VLP because its particle motions are most rectilinear and point to regions that intersect ~140 m below the station horizon (~300 m beneath the vent). This VLP depth is corroborated by the ~300 m deep sources found by *Sanderson et al.* [2010] for 2009 seismic data.

Though a robust moment tensor inversion is not possible with the sparse seismometer array, the VLP waveforms provide important constraints on the time history of source processes. We restitute vertical VLP displacement signals down to ~500 s and observe a temporary contraction (downward polarity) followed by recovery over the course of ~30 s (Figure 3). We propose that the onset of this wavelet corresponds to a failure of the reservoir and onset of gas advection upward toward the vent. Constrained by a consistent ~6 s time delay between VLP and explosion onsets, gas travels upward at an average speed of ~50 m/s.

We presume that loss of gas from a reservoir region leads to the detected deflation. If attributed to a simplistic isotropic point elastic source embedded within an elastic half-space, then the volumetric source strength is proportional to the surface deformation according to *Mogi* [1958]:

$$\Delta V = \frac{\pi r^2}{(1-\nu)} \left| \vec{u} \right|. \quad (1)$$

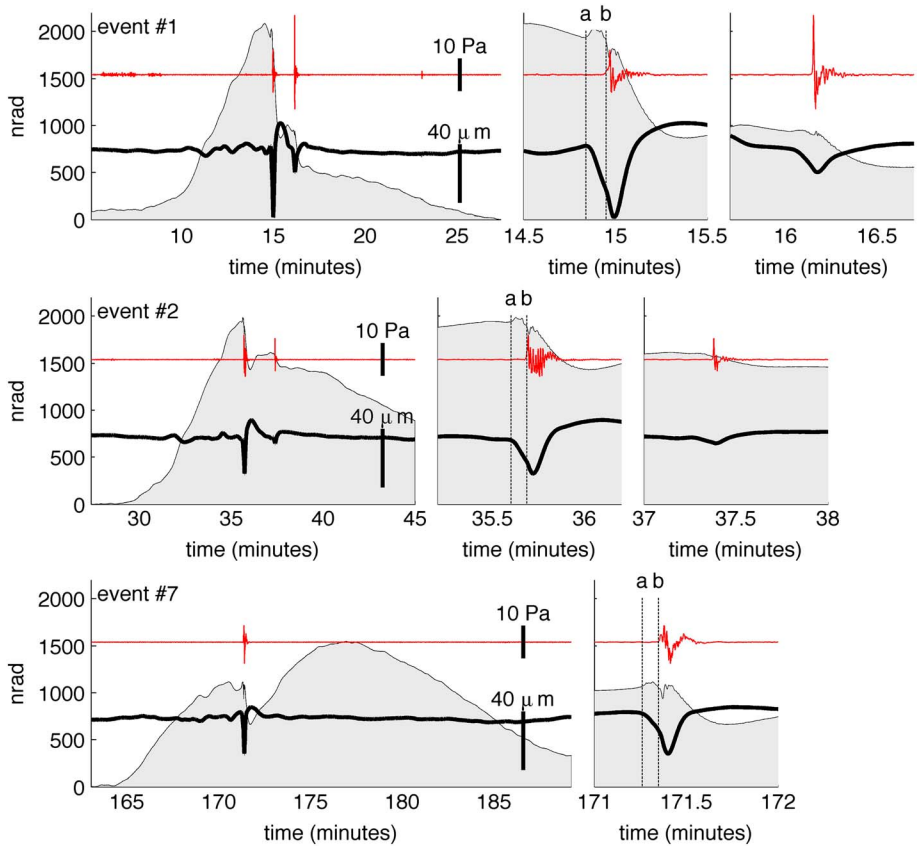

Figure 3. Minimum-phase (causally) filtered (below 60 s; grey) tilt and VLP seismic displacement signal (500 s to 2 s; black) from station #2 along with band-passed infrasound (10 s to 0.1 s; red) from station #3 for events shown in Figure 2. Detail of the explosion pulse shows the onset of the VLP (a) and subsequent onset of infrasound (b), which has been time shifted by ~1.5 s to account for propagation time. Relatively small high-frequency tilt transients, occurring at a and b, are response of tiltmeter to passing seismic and infrasound waves, respectively.

Assuming that the depressurization results primarily from gas evacuation, the ideal gas law is used to rewrite source strength in terms of gas mass loss,

$$\Delta m = P\frac{M}{RT}\frac{\pi r^2}{(1-\nu)}\left|\overrightarrow{u}\right|, \tag{2}$$

where Poisson's ratio $\nu = 0.25$, gas constant $R = 8.314$ J/mol/K, and gas is primarily water vapor at temperature $T = \sim 1200$ K with molar mass $M = 0.018$ kg/mol.

For reasonably large VLPs, such as event #1 of Figure 2, the peak displacement amplitude $\left|\overrightarrow{u}\right|$ is 10^{-4} m ($u_z = 0.4 \times 10^{-4}$ m) at a slant distance $r = 537$ m. The water mass loss responsible for the VLP would be ~2500 kg invoking a lithostatic pressure ($P = \sim 10$ MPa) approximation at 300 m (see Appendix A).

We compare this VLP-inferred volatile loss with coincident volume loss associated with the cyclic tilt, assuming that it too is generated by a Mogi-style point volume contraction at similar source depth. Given that Mogi tilt ω is related to the horizontal gradient of the vertical deformation by

$$\omega = \frac{(1-\nu)}{\pi}\frac{\Delta m RT}{MP}\frac{3xz}{(z^2+x^2)^{5/2}}, \tag{3}$$

associated mass loss is

$$\Delta m = P\frac{M}{RT}\frac{\pi}{(1-\nu)}\frac{(z^2+x^2)^{5/2}}{3xz}|\omega|. \tag{4}$$

Typical tilt cycle amplitudes at station #2 ($x = 518$ m and $z = 140$ m) are ~1.5 to 2 μrads, yielding ~$2–3 \times 10^4$ kg of inferred gas loss. The order-of-magnitude difference in source strength between VLP and tilt is reconciled because VLP represents rapid (tens of seconds) depressurization that is relatable to rapid initial gas mobilization, whereas tilt reflects a longer period (tens of minutes) transfer of gas through the upper edifice.

We emphasize that the tilt-inferred gas masses are lower estimates of the total mass fluxing through the volcano during each cycle. An equivalent strength Mogi source would induce less tilting if it was located shallower, or alternatively, much deeper within the edifice. Tilting would also be less significant for a volume source that is distributed or had a lozenge-shaped aspect [*Bonaccorso and Davis*, 1999]. Edifice loading and topography, which are not considered in this Mogi analysis, have second order influences on the surface tilt. The smallest possible volume source would occur for the situation where a Mogi point source depth is one half of the horizontal distance, i.e., $z = x/2 = 259$ m, to the tilt station. In this situation, the responsible gas mass loss would be 80% of the $2–3 \times 10^4$ kg cited above for a 140 m depth source.

A tilt-inferred gas mass exodus of ~$2–3 \times 10^4$ kg per 26 min cycle (or 12–18 kg/s) is compatible with measured SO_2 degassing rates of ~3 kg/s (peak during explosion) and ~1 kg/s (averaged over hours) [*Holland et al.*, 2011] because SO_2 represents a small percentage of the total volatile budget. Though H_2O/SO_2 ratios have not been directly measured at Santiaguito, typical ratios for arc volcanoes are on the order of 100 and can range from 10^1 to 10^3 [*Fischer*, 2008]. From the SO_2 fluxes in *Holland et al.* [2011] this implies that the total Santiaguito volatile flux could range from 10^1 to 10^3 kg/s, which is consistent with our tilt-inferred volatile fluxes.

Magma effusion rates also support the inferred 12–18 kg/s gas flux. The active lava flow of our study period suggests relatively high effusion rates within the bounds of the 0.1–0.7 m^3/s cited by *Harris et al.* [2002]. Invoking a lava flux of ~0.5 m^3/s (equivalent to 1250 kg/s for ~2500 kg/m^3 lava) would imply a volatile mass fraction n_f of 1.0 to 1.5%. This amount reflects gas segregation from the magma induced by decreasing solubility within the rising silicic melt. It is compatible with the ~1.6 to 2.4 wt % H_2O that is predicted to have been lost by the host magma by the time it has reached ~10 MPa (see Appendix A).

4. Eruption Controls

Analysis of a week-long population of tilt cycles sheds light upon the critical matter of what leads to explosive degassing, as opposed to passive venting (Figure 4). Of the 337 observed tilt cycles (averaging 26 ± 6 min), at least 73 are associated with VLPs and inferred explosion. Although the 26 min cycle time for the two populations exhibit no statistically significant difference (Figure 4h), we observe that a more rapidly tilting edifice has greater tendency to explode (Figure 4i); those events culminating in VLP have twice the average inflation rates of nonexplosive cycles. This occurs either because (1) the system is more quickly accumulating gas volume due to more rapid gas exsolution/expansion and/or (2) the gas flow is temporarily impeded at a depth, which enables efficient growth of a reservoir volume. We favor the latter mechanism because the stable 26 min cycle implies a quasi-steady rate of gas supply. The observation that few inflation cycles are shorter than ~20 min (Figure 4h) and that tilt amplitudes are similar further demonstrates a repeatable process, in which a minimum amount of gas must accumulate, prior to failure of the reservoir. We suggest that the two eruption modes, explosive versus nonexplosive, are affected by subtle differences in the geometry of the gas reservoir, which controls how normal stresses are transferred to, and open, a subvertical conduit.

5. Episodic Tilt at Other Volcanoes

Episodic inflation cycles are not unique to Santiaguito; however, their manifestation is distinct from those observed at episodically erupting volcanoes elsewhere. Both *Genco and Ripepe* [2010] and *Nishimura et al.* [2012] observed repeated gradual inflations tens to hundreds of seconds prior to coincident rapid deflation and explosions at Stromboli and Semeru (Indonesia). At these volcanoes the tilt cycles appear sawtooth shaped, occur nonperiodically, and are orders of magnitude smaller in amplitude than similarly proximal tilt recordings from Santiaguito. A further difference is that the Stromboli and Semeru tilt cycles uniformly culminated in explosions.

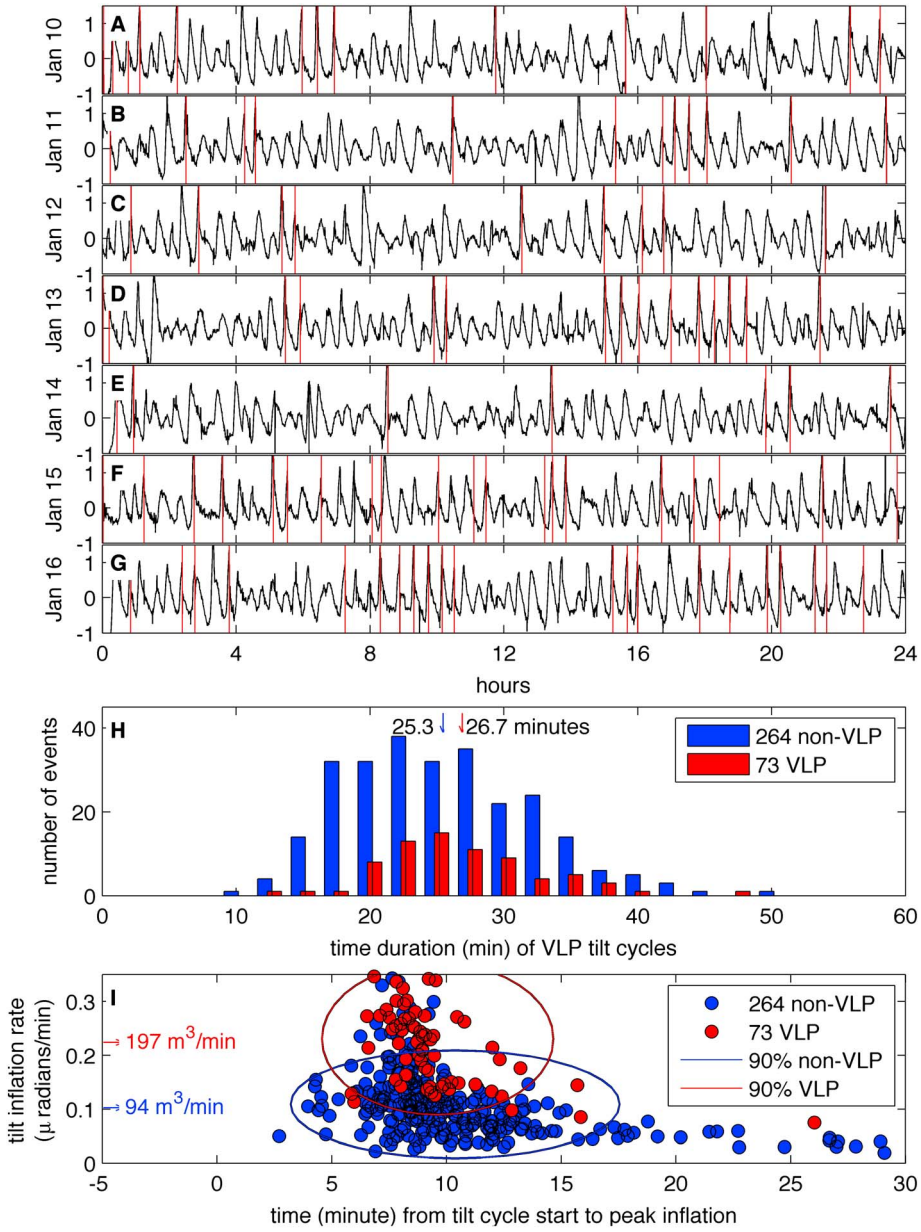

Figure 4. (a–g) Periodic tilt (measured in μrads) at station #2. Those events for which VLPs are detected are indicated with vertical red lines. (h) Histogram of tilt cycle period. (i) Faster tilt inflation rates are correlated with occurrence of VLP and explosions. Population median tilt values at station #2 are converted to responsible Mogi-source volume change rates (94 and 197 m^3/min) assuming a $z = 140$ m deep source region.

Santiaguito's sinusoidal tilt perhaps more closely resembles the character, including shape, periodic nature, and amplitude, of tilt recorded with similarly proximal tiltmeters near Soufrière Hills, albeit with significantly different time scale (4–30 h cycles [e.g., *Voight et al.*, 1999]). Soufrière Hills also differs in that inflation is accompanied by swarms of self-similar seismic events (families), which terminate as deflation begins [*Rowe et al.*, 2004]. Soufrière Hills's tilt cycles have been attributed to episodic stick/slip movement of a sticky magma column along conduit walls, for which deflation is correlated with slip events and surface dome growth [*Denlinger and Hoblitt*, 1999]. Tilt at Soufrière Hills has been attributed to vertical shear tractions, which episodically drag the edifice upward just prior to enhanced effusion [*Green et al.*, 2006].

The absence of both coinflation seismicity and of codeflation lava effusion is a significant observation at Santiaguito. The former observation indicates a lack of shear drag that results in stick/slip movement along

conduit margins, as proposed for Santiaguito by *Holland et al*. [2011]. The latter observation suggests tilt cycles driven primarily by nonsteady gas fluxing. Clearly, silicic magma rises and effuses at Santiaguito, but it appears to do so steadily and is not impeded by a plug of solidified lava, as is the proposed case at Soufrière Hills [*Green et al*., 2006]. Our observations are consistent with a continuously rising melt that feeds gas-charged regions as solubility drops. These gas reservoirs expand and pressurize the edifice. The gas reservoir reaches a critical pressure threshold, indicated by maximum tilt, prior to opening of the conduit and gas transit toward the vent. The critical pressure is controlled by the normal stresses acting on the fracture pathways and is likely affected by subtle variations in source depth and orientation of pathways. Observations presented here point to the importance of the free gas phase and its potential influence on the near-vent deformation field as previously proposed by *Nishimura* [2009].

6. Conclusion

Multiparameteric geophysical data from integrated seismoacoustic-tilt time series tell the chronology of gas accumulation and loss through the intermittently open-vent Santiaguito. Here regular inflation occurs as a consequence of gas exsolution and segregation, which pressurizes a region several hundred meters beneath the vent. Cyclic inflation is not correlated with pulses of lava effusion at the vent, but it is associated with degassing cycles.

Explosions tend to occur after relatively rapid inflation. An inward directed VLP, or contraction, heralds reservoir failure at ~300 m corresponding to a dramatic increase in conduit permeability and explosive eruptions from the vent ~6 s later. Passive degassing, on the other hand, occurs with slower rates of tilt and an absence of VLP signal, suggestive of a conduit that is less well sealed.

Periodic inflation of open-vent silicic volcanoes may be more common than previously appreciated. Observation of such signals at other volcanoes will require routine tilt monitoring closer to the conduit. Explosion occurrence at Santiaguito is modulated by inflation cycles, and this could well be the case elsewhere. If so, this hints at an exciting prospect for using near-field long-period deformations to foretell explosive events.

Appendix A: Information on Volatiles and Viscosity

Glass inclusion compositions were measured by electron microprobe using a JEOL 8900 Superprobe at the Smithsonian Institution Department of Mineral Sciences. Analyses were conducted using a 15 keV, 10 nA beam rastered over a 6 × 8 mm region. Data collection and analysis was performed with Probe for Electron Probe Micro-Analysis software; volatile loss was corrected using the self-volatile calibration. Standards used in analysis include glasses VG-99 and VG-568, fluorapatite, ilmenite, anorthoclase, augute, hornblende, microcline, scapolite, and pyrite; working standards include rhyolite glasses RLS132, VG568, and samples of RLS132 hydrated with 1–7 wt % H_2O. Inclusion size prevented analysis by Fourier transform infrared of most inclusions; those that were measured contain 0.5 to 1.2 wt % H_2O and no detected CO_2. The mean and standard deviation of 25 microprobe analyses is provided in the supporting information.

Glass inclusion data suggest ~2 wt % dissolved volatiles using the volatiles-by-difference method. The method of *Papale et al*. [2006] predicts equilibrium volatile solubility in the melt as a function of temperature, pressure, and melt composition. Differences between solubility at initial and final pressures provide an estimate of volatile loss during decompression. We assume an initial pressure of 75 to 100 MPa, corresponding to a depth of 3000 m, and a final pressure of 10 MPa, corresponding to a 300 m depth. We assume a magmatic temperature of 900–950°C, 60–70 vol % melt at the initial pressure, and a melt composition that matches the measured glass inclusions. Based upon those parameters and a pure H_2O volatile phase, the magma degassed ~1.6 to 2.4 wt % H_2O during decompression to 10 MPa. If a mixed CO_2-H_2O volatile phase is allowed (0.5 mol fraction H_2O), the model predicts ~1.0 to 1.5 wt % degassing. Note that magma likely contained a minimum of 4 wt % H_2O at depth as indicated by the presence of hornblende and work by *Scott et al*. [2012]; thus, these degassing estimates are minimum values.

Melt viscosity is calculated using the method of *Giordano et al*. [2008]. Applying that model to measured glass compositions at temperatures of 900–950°C, we calculate viscosities of $10^{5.3}$–$10^{5.8}$ Pa s at 100 MPa (~3.5 wt % dissolved H_2O), $10^{5.5}$–$10^{6.0}$ Pa s at 75 MPa (~3 wt % dissolved H_2O), and $10^{6.4}$–$10^{7.0}$ Pa s at 10 MPa (~1 wt %

dissolved H_2O). Bulk magma viscosity, m_M, can be estimated with the Einstein-Roscoe equation that accounts for the effects of solid (nondeforming) phases within the melt:

$$\mu_M = \mu_0 \left(1 - \frac{\phi}{\phi m}\right)^{-\frac{5}{2}} \tag{A1}$$

where m_o is the melt viscosity, f is the calculated crystal fraction, and f_m is the crystal fraction at which the system locks (assumed to be 40% total crystals). Assuming crystallinity of 30 vol %, we calculate bulk viscosities of $10^{6.8}$–$10^{7.3}$ Pa s at 100 MPa, $10^{7.0}$–$10^{7.5}$ Pa s at 75 MPa, and $10^{7.9}$–$10^{8.5}$ Pa s at 10 MPa. These values are compatible with those cited in viscosity modeling by *Holland et al.* [2011].

Given these viscosity values, it is possible to estimate driving pressures of the magma conduit at depth. We suppose that slow rise of magma is characterized as Poisseulle flow, where pressure gradient above lithostatic is

$$\frac{dP}{dz} = \frac{8\mu Q}{\pi r^4} \tag{A2}$$

where μ is dynamic viscosity (10^7 to 10^8 Pa s), Q is volumetric flux (0.1 to 0.7 m^3/s [*Harris et al.*, 2002]), and r is pipe (or conduit) radius (18 m from *Holland et al.* [2011]). Giving these constraints the pressure gradient required to drive magma upward will be 10^1 to 10^3 Pa/m, which is only a fraction of the ~$10^{4.5}$ Pa/m lithostatic gradient. We conclude that pressure conditions in the conduit, including gas reservoir regions, are thus approximately lithostatic.

Acknowledgments

We thank INSIVUMEH, the Policia Nacional Civil de Guatemala, and the Instituto Guatemalteco de Turismo for support. Fieldwork was carried out with support from Armando Pineda and Jake Anderson. The project was supported by a grant from the National Science Foundation (EAR 0838562) and a Smithsonian Natural History Museum Small Grant. We thank IRIS PASSCAL for hardware support. Santiaguito seismic data are available from the IRIS DMC.

The Editor thanks two anonymous reviewers for their assistance in evaluating this paper.

References

Bluth, G. J. S., and W. I. Rose (2004), Observations of eruptive activity at Santiaguito volcano, Guatemala, *J. Volcanol. Geoth. Res.*, *136*(3-4), 297–302, doi:10.1016/j.jvolgeores.2004.06.001.

Bonaccorso, A., and P. M. Davis (1999), Models of ground deformation from vertical volcanic conduits with application to eruptions of Mount St. Helens, *J. Geophys. Res.*, *104*(B5), 10,531–10,542, doi:10.1029/1999JB900054.

Denlinger, R. P., and R. P. Hoblitt (1999), Cyclic eruptive behavior of silicic volcanoes, *Geology*, *27*, 459–462, doi:10.1130/0091-7613(1999)027<0459:CEBOSV>2.3.CO;2.

Fischer, T. P. (2008), Fluxes of volatiles (H_2O, CO_2, N2, Cl, F) from arc volcanoes, *Geochem. J.*, *42*, 21–38.

Genco, R., and M. Ripepe (2010), Inflation-deflation cycles revealed by tilt and seismic records at Stromboli volcano, *Geophys. Res. Lett.*, *37*, L12302, doi:10.1029/2010/GL042925.

Giordano, D., J. K. Russell, and D. B. Dingwell (2008), Viscosity of magmatic liquids: A model, *Earth Plane. Sci. Lett.*, *271*, 123–134, doi:10.1016/j.epsl.2008.03.038.

Green, D. N., J. Neuberg, and V. Cayol (2006), Shear stress along the conduit wall as a plausible source of tilt at Soufriere Hills volcano, Montserrat, *Geophys. Res. Lett.*, *33*, L10306, doi:10.1029/2006GL025890.

Harris, A. J. L., W. I. Rose, and L. Flynn (2002), Temporal trends in lava dome extrusion at Santiaguito 1922-2000, *Bull. Volcan.*, *65*, 77–89, doi:10.1007/sO04556-002-0243-0.

Holland, P. A. S., M. I. Watson, J. C. Phillips, L. Caricchi, and M. P. Dalton (2011), Degassing processes during lava dome growth: Insights from Santiaguito lava dome, Guatemala, *J. Volc. Geotherm. Res.*, *202*, 153–166, doi:10.1016/j.jvolgeores.2011.02.004.

Johnson, J. B., J. M. Lees, A. Gerst, D. Sahagian, and N. Varley (2008), Long-period earthquakes and co-eruptive dome inflation see with particle image velocimetry, *Nature*, *456*, 377–381, doi:10.1038/nature07429.

Johnson, J. B., B. J. Andrews, and J. M. Lees (2013), Flow, bulge, and jerk; quantifying surface motions with particle image velocimetry at Volcan Santaiguito (Guatemala) Abstract V52C-07, presented at 2013 Fall Meeting, AGU, San Francisco, Calif., 9-13 Dec.

Mogi, K. (1958), Relations between the eruptions of various volcanoes and the deformation of the ground surfaces around them, *Bull. Earthquake Res. Inst. U. Tokyo*, *36*, 99–134.

Neuberg, J., and T. Pointer (2000), Effects of volcano topography on seismic broad-band waveforms, *Geophys. J. Int.*, *143*, 239–248, doi:10.1046/j.1365-246x.2000.00251.x.

Neuberg, J., R. Luckett, M. Ripepe, and T. Braun (1994), Highlights from a seismic broadband array on Stromboli volcano, *Geophys. Res. Lett.*, *21*(9), 749–752, doi:10.1029/94GL00377.

Nishimura, T. (2009), Ground deformation caused by magma ascent in an open conduit, *J. Volcanol. Geotherm. Res.*, *187*, 178–192, doi:10.1016/j.jvolgeores.2009.09.001.

Nishimura, T., M. Iguchi, R. Kawaguchi, H. H. Surono, and U. Rosadi (2012), Inflations prior to Vulcanian eruptions and gas bursts detected by tilt observations at Semeru Volcano, Indonesia, *Bull. Volcan.*, *74*, 903–911, doi:10.1007/s00445-012-0579-z.

Papale, P., R. Moretti, and D. Barbato (2006), The compositional dependence of the saturation surface of $H_2O + CO_2$ fluids in silicate melts, *Chem. Geol.*, *229*, 78–95, doi:10.1016/j.chemgeo.2006.01.013.

Rose, W. I. (1987), Volcanic activity at Santiaguito Volcano, 1976-1984, *Geol. Soc. Am.*, *212*, 17–27, doi:10.1130/SPE212-p17.

Rowe, C. A., R. C. Aster, P. R. Kyle, J. W. Schlue, and R. R. Dibble (1998), Broadband recording of Strombolian explosions and associated very-long-period seismic signals on Mount Erebus volcano, Ross Island, Antarctica, *Geophys. Res. Lett.*, *25*, 2297–2300, doi:10.1029/98GL01622.

Rowe, C. A., C. H. Thurber, and R. A. White (2004), Dome growth behavior at Soufriere Hills Volcano, Montserrat, revealed by relocation of volcanic event swarms, 1995-1996, *J. Volcanol. Geotherm. Res.*, *134*(3), 199–221, doi:10.1016/j.jvolgeores.2004.01.008.

Sahetapy-Engel, S., A. J. L. Harris, and E. Marchetti (2008), Thermal, seismic and infrasound observations of persistent explosive activity and conduit dynamics at Santiaguito lava dome, Guatemala, *J. Volcanol. Geotherm. Res.*, *173*, 1–14, doi:10.1016/j.jvolgeores.2007.11.026.

Sanderson, R., J. B. Johnson, and J. M. Lees (2010), Ultra-long period seismic signals and cyclic deflation coincident with eruptions at Santiaguito volcano, Guatemala, *J. Volcanol. Geotherm. Res.*, *198*, 35–44, doi:10.1016/j.jvolgeores.2010.08.007.

Scott, J. A. J., T. A. Mather, D. M. Pyle, W. Rose, and G. Chigna (2012), The magmatic plumbing system beneath Santiaguito Volcano, Guatemala, *J. Volcanol. Geotherm. Res.*, *327-328*, 54–68, doi:10.1016/j.jvolgeores.2012.05.014.

Scott, J. A. J., D. M. Pyle, T. A. Mather, and W. I. Rose (2013), Geochemistry and evolution of the Santiaguito volcanic dome complex, Guatemala, *J. Volcanol. Geotherm. Res.*, *252*, 92–107, doi:10.1016/j.jvolgeores.2012.11.011.

Siebert, L., and T. Simkin (2002), Volcanoes of the world: An illustrated catalog of Holocene volcanoes and their eruptions, Global Volcanism Program, Digital Information Series GVP-3, Smithsonian Institution, Washington, D. C.

Voight, B., et al. (1999), Magma flow instability and cyclic activity at Soufriere Hills Volcano, Montserrat B.W.I, *Science*, *283*(5405), 1138–1142, doi:10.1126/science.283.5405.1138.